Author(s): Kivisaari, Pyry & Kim, Iurii & Suihkonen, Sami & Oksanen, Jani

Title: Elimination of Lateral Resistance and Current Crowding in Large-Area LEDs by Composition Grading and Diffusion-Driven Charge Transport

Year: 2017

Version: Post print

Please cite the original version:

Kivisaari, Pyry & Kim, Iurii & Suihkonen, Sami & Oksanen, Jani. 2017. Elimination of Lateral Resistance and Current Crowding in Large-Area LEDs by Composition Grading and Diffusion-Driven Charge Transport. Advanced Electronic Materials. Volume 3, Issue 6. 1700103. 2199-160X (printed). DOI: 10.1002/aelm.201700103.

Elimination of lateral resistance and current crowding in large-area LEDs by composition grading and diffusion-driven charge transport

Pyry Kivisaari[3], Iurii Kim[2], Sami Suihkonen[2] and Jani Oksanen[1⋆]
[1]*Engineered Nanosystems Group, Aalto University, P.O. Box 12200, FI-00076 Aalto, Finland,* [2]*Department of Micro- and Nanosciences, Aalto University, P.O. Box 13000, FI-00076 Aalto, Finland and* [3]*Division of Solid State Physics and NanoLund, Lund University, P.O. Box 118, SE-22100 Lund, Sweden*

Gallium nitride based light-emitting diodes (LEDs) are presently fundamentally transforming the lighting industry, but limitations in the materials and fabrication methods of LEDs introduce substantial challenges to their future development. Among the remaining key bottlenecks of GaN LEDs are the resistive losses and current crowding that strongly increase the heat generation at high powers. In this work we show how a new design paradigm based on diffusion-driven charge transport (DDCT) and selective-area growth (SAG) of GaN could be used to reduce the resistive losses of LEDs below the level achievable with presently available structures. We carry out full device simulations and demonstrate SAG of both n- and p-doped GaN on device templates with InGaN quantum wells that can be excited using DDCT. Our results indicate that especially when combined with material composition grading, the new approach offers the possibility to substantially reduce the resistive heating in high-power LEDs.

—Preprint of the article published in Advanced Electronic Materials, p. 1700103, Apr. 2017
http://doi.wiley.com/10.1002/aelm.201700103—

After two decades of very successful technology development, white light-emitting diodes (LEDs) are quickly replacing traditional light sources and enabling substantial reductions in global energy consumption [1]. Despite the progress, however, LEDs still have plenty of room for improvement especially in high-power lighting applications. The most well-known scientific and technological challenge for gallium nitride (GaN) based LEDs is without a doubt the strong reduction of the quantum efficiency, i.e. the efficiency droop, at high input powers [2, 3]. A less widely studied but technologically an almost equally important related performance limitation is introduced by the resistive loss, current crowding and Joule heating especially in the n-type current-spreading layer (CSL) of conventional LEDs at high input powers [4–7]. These limitations fundamentally arise from the resistance of the CSL, and they also reduce the effective area of the ohmic contacts and further aggravate the droop.

To mitigate the effects of the resistive losses, Hurni *et al.* recently showed that increasing the thickness of the n-type CSL leads to significantly less pronounced current crowding and improves the wall-plug efficiency of LEDs at large currents [8]. However, this approach still necessitates using expensive bulk GaN substrates and a part of the active region (AR) needs to be cut out to deposit n-type contacts, exposing the edges of the AR to surface recombination. The basic structure of Hurni's low resistance LEDs as well as essentially all conventional LEDs relies on a double heterojunction (DHJ) design, where electrons and holes are injected to the AR from n- and p-doped regions located on the opposite sides of the AR. This sets evident limitations to designing the structures so that the contacts do not substantially decrease the total AR area or increase the free surface area susceptible to surface recombination. To avoid some of the limitations of conventional DHJ structures related to device scaling, resistive losses and electrical excitation in general, diffusion-driven charge transport (DDCT) was very recently introduced as an alternative way to electrically excite the AR of LEDs [9–12]. In DDCT, the pn junction is partly separated from the AR, and in contrast with conventional solutions it relies on transporting electrons and holes to the AR from the same side by bipolar diffusion, enabling additional degrees of freedom for designing new devices.

For practical reasons, the previous works on DDCT have mainly focused on structures containing vertically formed pn-homojunctions, which entail potential barriers and lead to suboptimal device performance. In this paper, however, we show that the electrical inefficiencies observed earlier can be fully eliminated by adapting the DDCT concept to realize laterally doped heterojunction (LHJ) structures (see Fig. 1), and that the selective area growth (SAG) techniques needed to realize such LHJ devices do not compromise the internal quantum efficiency of the AR. Furthermore, our results show that the LHJ structures can be further engineered using appropriate material composition gradings, that can reduce the resistive heating of the devices even below the limit set by ideal conventional DHJ devices.

The fundamental difference between the DHJ and LHJ structures is the placement and geometry of the doped p- and n-GaN charge injection regions, which are expected to mainly affect charge transport and injection efficiency of the structures. To illustrate the possibilities offered by DDCT in improving the performance of high power LEDs, we carry out full-device simulations of the electrical properties of selected variants of the DHJ and LHJ structures shown in Fig. 1. The figure shows the

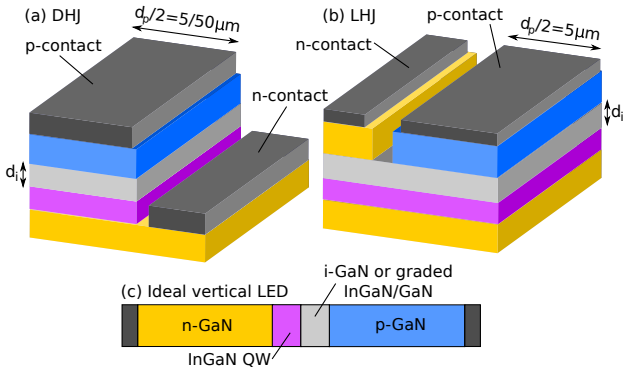

FIG. 1: Schematic illustration of the finger structure in (a) conventional planar DHJ InGaN/GaN QW LED where n-type contacts are fabricated by piercing through the active region, typically occupying ca. 10 % of the chip area. (b) Lateral heterojunction (LHJ) diffusion-driven LED, where the doped regions are created by selective-area growth of a repeating array of 3 μm wide n-GaN and 10 μm wide p-GaN stripes. (c) Ideal vertical LED with perfect contacts covering both p- and n-surfaces so that the device is essentially 1-dimensional and lateral current spreading is not present. The structures in (a) and (b) only show one half of the structure; the full structure is obtained by mirroring with respect to the leftmost sidewall.

schematic cross-section of (a) a conventional planar DHJ-based LED, where the n-contacts are realized as contact fingers piercing through the AR, and where light is extracted through the substrate (not shown) [13], (b) an LHJ structure, where narrow p- and n-doped regions are fabricated side by side on one side of the AR using SAG, so that electrons and holes can flow to the AR through bipolar diffusion, and (c) the ideal vertical DHJ LED structure where perfect (transparent) contacts cover both the bottom and the top of the essentially 1-dimensional structure that provides an ideal reference structure where no lateral current transport or lateral losses take place. This structure also well corresponds to the limit, where the width of the DHJ structure in Fig. 1(a) approaches zero when surface recombination is not considered, and will therefore be denoted as structure DHJ-0 in the following.

In addition to studying the piecewise homogeneous structures, we also compare them to structures where the GaN interlayer (thickness d_i) blocking Mg diffusion to the QW during growth [14] has been replaced by a 100 nm thick linearly graded $In_{7.5}Ga_{92.5}N$-GaN material layer where the n-type polarization doping [15] is fully neutralized by an equivalent p-type impurity doping. For simplicity, the AR consists of a single $In_{15}Ga_{85}N$ QW in all the structures, the contact separation between the n- and p-type contacts is set to 1 μm and the total width of the n-contact fingers of the DHJ structures is 10 % of the p-contact width d_p. In the LHJ structures, the n- and p-GaN layer widths are $d_n = 3$ and $d_p = 10$ μm, respectively. The n- and p-layer thickness in all the LHJ structures is 150 nm, and the same thicknesses are also

TABLE I: Main parameters defining the simulated structures analyzed in Figs. 2-4. In the graded structure (denoted with the postfix G) the $In_{7.5}Ga_{92.5}N$ to GaN grading takes place over a 100 nm thick polarization doping compensated layer above the QW. Structures marked with parentheses have also been simulated, but their main features are only discussed in the text to keep the figures more tractable.

DHJ			DHJ-G			LHJ		
	d_p	d_i		d_p	d_i		d_p	d_i
	μm	nm		μm	nm		μm	nm
DHJ-0	0	10	DHJ-0G	0	100	LHJ-G	10	100
DHJ-10	10	10	(DHJ-10G)	10	100	LHJ-10	10	10
DHJ-100	100	10	(DHJ-100G)	100	100	LHJ-50	10	50

used for the ideal 1-dimensional DHJ reference structures to ensure the least amount of resistive losses. In the truly 2-dimensional DHJ structures, the n-layer thickness has been increased to 2 μm, corresponding to realistic state-of-the-art LEDs to enable more realistic current spreading. The other details of the simulated structures as well as the naming convention used to identify the devices and their dimensions have been presented in Table I.

To investigate and compare the operation of the DHJ and LHJ structures described in the previous paragraphs, we solve the standard drift-diffusion model relating the electrostatic potential ϕ and the electron and hole current densities $\mathbf{J}_n, \mathbf{J}_p$ to the electron and hole densities p and n, the ionized donor and acceptor densities N_d and N_a, the polarization density $\mathbf{P}_{tot}$ consisting of spontaneous and piezoelectric polarization and the conduction and valence band quasi-Fermi levels E_{Fn} and E_{Fp} as well as the net recombination rate density R [16]. Quantitatively the drift-diffusion model is given by

$$\begin{aligned} \nabla \cdot (-\varepsilon \nabla \phi) &= e\,(p - n + N_d - N_a) - \nabla \cdot \mathbf{P_{tot}} \\ \nabla \cdot \mathbf{J}_n &= \nabla \cdot (-e\mu_n n \nabla \phi_n) = eR \\ \nabla \cdot \mathbf{J}_p &= \nabla \cdot (-e\mu_p p \nabla \phi_p) = -eR, \end{aligned} \tag{1}$$

where ε is the static permittivity, e is the elementary charge, and μ_n, μ_p are the electron and hole mobilities. The ionized acceptor density is calculated using Fermi-Dirac distribution with an acceptor ionization energy of 170 meV similarly as in Ref. [11]. The simulations are carried out as 2D simulations describing the cross-section of the devices perpendicular to the contact fingers. To account e.g. for the strong quantum confined Stark effect in the QWs, we solve the QW envelope wavefunctions from the effective mass Schrödinger equation in the QW for the lowest-lying confined states based on the QW electric field given by Poisson's equation and use them to calculate the recombination rates. For all recombination processes, we also follow the scaling proposed in Ref. [17], meaning that the 2D recombination rate densities are scaled by the overlap integral of the electron and hole ground states. While considerable uncertainty

generally surrounds the quantitative description of optical and electrical properties of III-N QWs (see, e.g., Refs. [18–20]), such uncertainties do not significantly affect the main conclusions of this paper due to the comparative nature of the simulations and since our results mainly focus on the charge transport in the bulk layers. For the surface recombination at the edges of the DHJ active region we employ the simple surface recombination model based on Ref. [21] with recombination rate given by $R_s = v_s(np - n_i^2)/(n + p + 2n_i)$, where n_i is the intrinsic carrier density of the QW and the surface recombination velocity is $v_s = 3 \times 10^4$cm/s [22]. The donor and acceptor densities of the n- and p-GaN layers are set to 5×10^{18} cm^{-3} and 1×10^{19} cm^{-3}, and the electron and hole mobilities are 230 cm^2/(Vs) and 10 cm^2/(Vs) for the doped layers, respectively, based on our previous Hall measurements. Electron and hole mobilities in the unintentionally doped GaN are set to 1000 cm^2/(Vs) and 70 cm^2/Vs based on the calculations reported in Ref. [23]. The recombination parameters were chosen as $A = 10^7$ 1/s, $B = 5 \cdot 10^{-17}$ m^3/s and $C = 10^{-42}$ m^6/s, similar to Ref. [24].

Figure 2(a) shows the bias voltages V needed to drive selected LEDs of Table I as a function of the current density. The current densities are calculated by dividing the total current with the total device area to also account for the n-contact areas of the DHJ structures. Fig. 2(a) shows that, somewhat unexpectedly, the idealized vertical DHJ structure (DHJ-0) does not provide the absolute lower limit for the device performance, but it can be further improved by introducing a suitable material grading next to the AR as in the structure LHJ-G. This is evidenced in the figure by the smaller bias voltage needed to reach the same current densities as in the DHJ-0 reference structure. A nearly identical improved JV behaviour (not shown) is also found for structure DHJ-0G. In addition, the ungraded LHJ-10 structure performs nearly as well as the DHJ-0 structure. The other LHJ and DHJ devices with larger i-GaN spacer layer thicknesses d_i or larger DHJ p-contact widths d_p, on the other hand, exhibit substantially larger voltages at high current densities even in the case of the graded DHJ structures.

Figure 2(b) shows the specific differential resistances of the devices as a function of the current density. Broadly speaking, the differential resistances of the simulated structures can be divided in two categories: 1) the 'low' differential resistance group with the resistance decreasing below 2×10^{-4} Ωcm^2 at the largest current densities and 2) the 'high' resistance group with differential resistances that are clearly larger than the resistance of the DHJ-0 reference structure. The low resistance group includes all the simulated LHJ structures but only the idealized DHJ structure DHJ-0, suggesting that using the LHJ structures indeed works as an effective way to reduce ohmic heating of the structures. In addition, the differential resistances of structures DHJ-10 and DHJ-10G also approach the low differential resistance category (not shown), but due to considerable surface recombination losses they are not as efficient as the other structures. All the performed simulations additionally suggest that grading only modestly affects the differential resistance.

To illustrate how differences in the lateral current spreading affect the electrical performance we evaluate the electrical efficiency as $\eta_{ele} = \hbar\omega R/(UJ)$ where $\hbar\omega = 2.85$ eV is the average energy released in a recombination process and R is the total recombination rate per unit area within the active region. In essence, this ratio gives a parametrized figure of merit for the electrical efficiency; when a current corresponding to an overall recombination rate R flows to the AR, η_{ele} describes the ratio of the power dissipated in the active region to the input power. Figure 2(c) shows the electrical efficiency as a function of current density, indicating that the electrical efficiency of the graded structure LHJ-G can be notably larger than in the DHJ-0 structure because the grading lowers the height of the potential barriers the carriers encounter when they are transported to the AR. A similar but slightly less pronounced effect can also be observed in the ideal vertical DHJ-0G structure (not shown), which, however, cannot be straightforwardly realized with presently available contact materials. Also the LHJ-10 structure exhibits only slightly lower efficiency than the DHJ-0 structure. In contrast, all studied ungraded conventional DHJ structures exhibit significantly smaller electrical efficiency due to larger electrical losses and/or surface recombination. This indicates that combining DDCT with composition grading can substantially increase the electrical efficiency of LEDs at all relevant current densities. In addition, at small currents the electrical efficiency can increase to above 100% when the electrons and holes capture energy from the lattice heat, transferring it to the electrons and holes at the active region. For sufficiently high efficiency LEDs the associated heat absorption can be even larger than the heat generation by all other loss mechanisms together, leading to the possibility of electroluminescent cooling [25]. For DHJ-0 the heat absorption can completely overshadow the resistive heating up to current densities of the order of 50A/cm^2. For structure LHJ-G the point where resistive losses equal the heat absorption is moved to four times larger current densities, suggesting that with further development the LHJ structures could provide a feasible pathway for extending the conventionally narrow operating regime where the bias voltage is in fact lower than the voltage corresponding to the energy of the emitted photons, observed e.g. in the IV-curve of Ref. [8]. Extending this regime to higher current densities might provide the necessary advances to harness the thermoelectric cooling effect in developing more efficient LEDs [26, 27] or even electroluminescent cooling [28, 29].

Figure 3 additionally shows the (a) IQE and (b) WPE extracted from the simulations for selected structures. In Fig. 3(a), the IQEs are nearly equal for all other structures than DHJ-10 with large surface recombination, suggesting that the AR carrier distributions behave very similarly as a function of the current density in all of

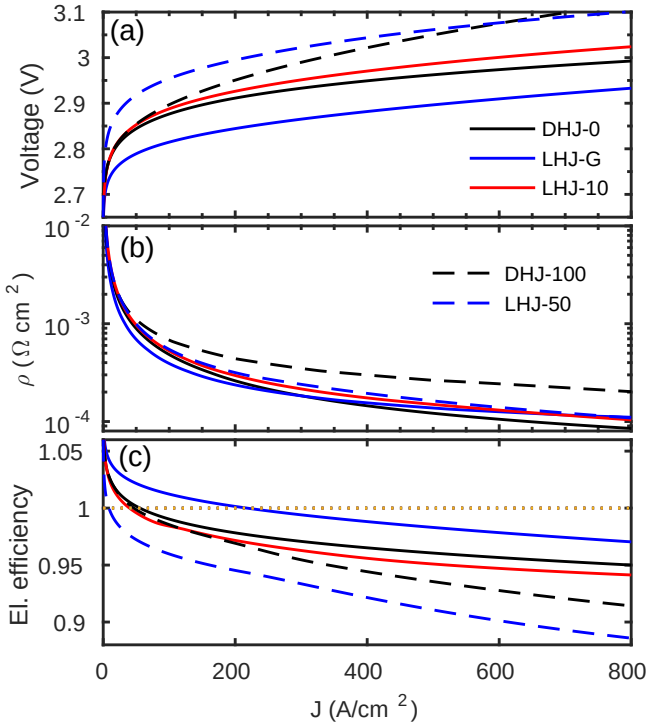

FIG. 2: (a) The bias voltage, (b) differential resistance and (c) electrical efficiency of selected structures as a function of the current density. The legends are shared between the figure panels and the dotted line in (c) denotes the unity efficiency.

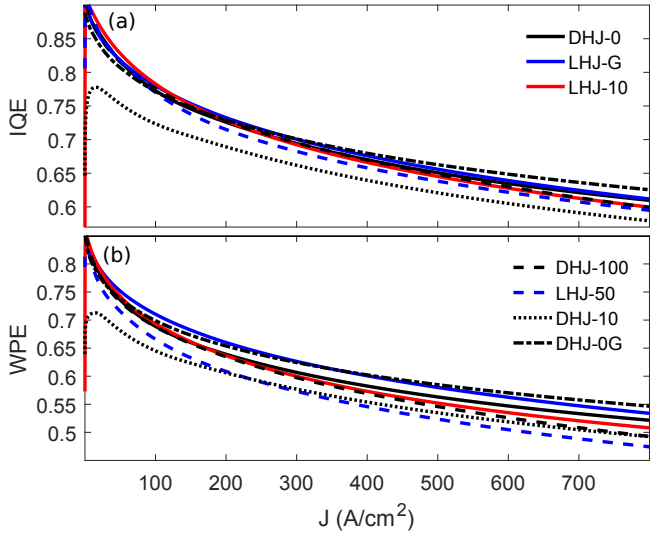

FIG. 3: (a) Internal quantum efficiency and (b) wall-plug efficiency extracted from the simulations.

the structures. On the other hand, Fig. 3(b) shows that the differences in the electrical performance also lead to additional differences in the WPEs between the structures. Due to its smallest overall electrical loss as observed in Fig. 2(c), the LHJ-G structure has the highest WPE, even higher than that of the ideal vertical DHJ-0 structure. The LHJ-10 and DHJ-100 structures both have slightly lower WPEs than the DHJ-0 structure at large currents due to their larger electrical losses. The LHJ-50 structure has the lowest WPE due to the diffusion loss in its 50nm thick intrinsic GaN layer, even when it has an injection efficiency (not shown) of at least 98 % throughout the studied current density range. All the other structures have injection efficiencies even closer to unity. Overall, Fig. 3 clearly shows that in addition to having better electrical performance (Fig. 2) the LHJ structures have also equal or better optical performance as the DHJ structures even with the single QW structure studied here. For MQW structures or thick active region devices enabling larger current densities with a high IQE, however, the improvement in the WPE is expected to become more pronounced in the LHJ structures due to their improved electrical properties at high currents.

To further quantify the inherent differences in the current spreading of the devices, we have analyzed the uniformity of the recombination in the studied structures. In general the recombination profile becomes more uniform as the width of the structures is decreased. In practice, however, the lower limits for decreasing the widths are set by the use of optical lithography (LHJ) for fabricating the devices and the increase of surface recombination (DHJ) starting to notably reduce the device efficiency below approximately 100μm stripe widths. Fig. 4 shows the 2-dimensional recombination rate densities in the best performing DHJ and LHJ devices LHJ-G, LHJ-10 and DHJ-100 (a) at relatively strong injection around 200 A/cm^2 and (b) at very strong injection around 400 A/cm^2. The common x-axis is chosen so that it spans the full width of the DHJ-100 AR and the n-contact (112 μm), and the recombination profiles of the more narrow structures are repeated periodically. The gray background indicates the n-doped regions of the LHJ structures, and the 1 μm wide openings between the n- and p-regions. The grading has only a minor effect on the spatial distribution of recombination, presumably resulting from slight differences in the vertical carrier density profiles of the structures and small differences in the exact current densities resulting from the calculation grid. The difference between the DHJ and the LHJ structures, on the other hand is very clear. In the LHJ structure the spatial decay of the recombination is governed by the carrier diffusion lengths, which lead to fast decay of the hole population and recombination rate under the n-contacts due to the small hole mobility and much slower decay under p-contacts due to the relatively large electron mobility. In the DHJ structure the decay length is mainly determined by the resistance of the n-GaN CSL, leading to slower but strongly current density dependent decay.

A closer inspection of the recombination distribution of Fig. 4(a) shows that at 200 A/cm^2 the spatial averages of the recombination rate in the LHJ and DHJ structures are approximately 0.7 and 0.55 of the corresponding peak values. Since the peak values correspond to the largest

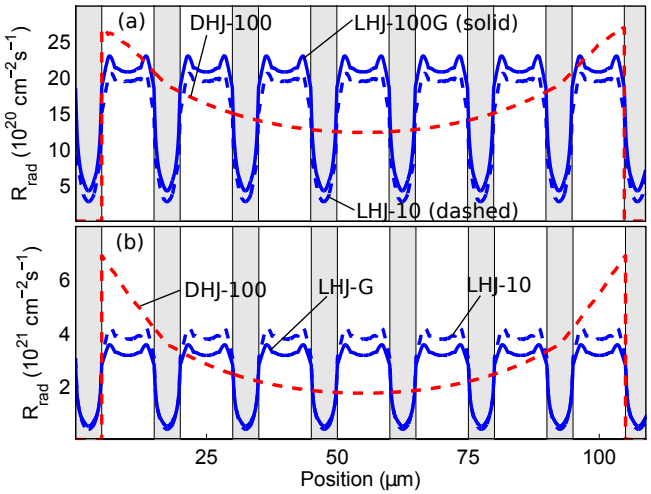

FIG. 4: Recombination rate density as a function of position in the best 2-dimensional device classes (DHJ-100, LHJ-10 and LHJ-G) for (a) relatively strong injection with a current density of ∼200 A/cm^2 and (b) very strong injection with a current density of ∼ 400 A/cm^2. The gray background indicates the n-doped regions of the LHJ structures and the 1 μm wide openings between the n- and p-regions. The zero recombination in the DHJ structures corresponds to the n-contact fingers, which pierce the AR.

possible rate for the applied bias voltage and the average value corresponds to the injected current, this indicates more efficient charge spreading in the LHJ structure. The difference between the LHJ and DHJ structures is even larger in Fig. 4(b), where the same curves are plotted for current density 400 A/cm^2. The spatial averages are approximately 0.65 of the maximum value for the LHJ structures and below 0.45 for the DHJ structure. This clearly also indicates that current spreading in the LHJ scheme depends much less strongly on the current density than in the DHJ scheme. In addition, we expect that further engineering the contact widths and the properties of the diffusion layer for the asymmetric properties of electrons and holes can lead to larger average values for the graded LHJ structures than obtained for the prototype structures studied here.

The proposed lateral DDCT scheme depends on the ability to fabricate closely spaced lateral n- and p-type GaN regions. To demonstrate the general feasibility of the SAG process for this purpose, we fabricated separately grown n- and p-type GaN layers using metalorganic vapor-phase epitaxy (MOVPE) on SiO_2 patterned device templates. The templates consist of a 5 um thick unintentionally doped intrinsic GaN (i-GaN) as the buffer layer on a c-plane sapphire substrate, on top of which a standard 5 well InGaN/GaN MQW active region is grown, followed by a 120 nm i-GaN capping. The precursors for the growth were trimethyl gallium (TMG), trimethyl indium (TMI), and trimethyl aluminium (TMA). A 100 nm thick SiO_2 SAG mask was

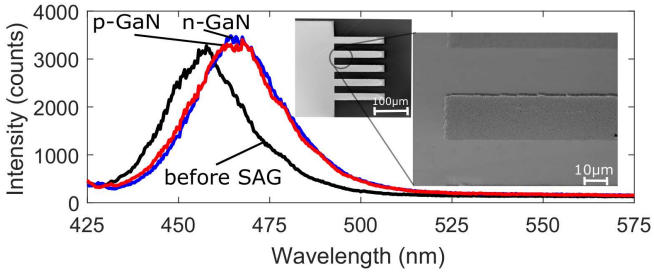

FIG. 5: Photoluminescence spectra before and after the SAG of n-GaN and p-GaN layers on the device templates. The inset shows a SEM image of the n-type finger pattern fabricated using SAG. The small shift in the PL peak position is expected to result from run to run variations between the templates.

subsequently deposited on the templates using PECVD and patterned using standard lithography techniques to suppress the growth of GaN elsewhere than in the openings defined in the SiO_2 layer [30]. After patterning, 150 nm SAG n-GaN or p-GaN layers were grown on top of the template. The quality and morphology of the layers grown by SAG was investigated by scanning electron microscopy (SEM) and photoluminescence (PL) measurements comparing the PL signal of the templates before and after SAG growth. Fig. 5 shows the photoluminescence (PL) from the samples excited using a pump laser at 405 nm before and after SAG of p- and n-type GaN. Based on the PL measurements SAG does not notably affect the luminescence from the MQW, suggesting that SAG provides a promising method to fabricate laterally doped GaN devices. The scanning electron microscope (SEM) images of the structures additionally show that the SiO_2 mask is able to well define the growth areas. While the edges of the SAG regions typically grow faster than the middle parts due to diffusion of the precursor materials on the surface of SiO_2 [31], this is not expected to present a major problem as long as the MQW quality is not compromised.

In conclusion, we compared the lateral current spreading and current crowding properties of high power GaN LEDs based on conventional DHJ structures as well as LEDs based on the recently introduced DDCT principle. Our results suggest that laterally doped DDCT LEDs can clearly outperform conventional DHJ devices, and that material grading could improve their performance even beyond the ideal DHJ structures whose fabrication is not feasible with the presently available materials compatible with GaN. In addition, we showed that the selective-area growth of GaN needed to realize the studied DDCT devices in practice does not deteriorate the photoluminescence from the QW templates, indicating that SAG provides a viable pathway to fabricating the first DDCT based high power LEDs.

Acknowledgments: Financial support from the Nokia Foundation, Emil Aaltonen Foundation and Walter Ahlström Foundation, Academy of Finland and the European Research Council through the European Unions

Horizon 2020 Research and Innovation Programme under Grant 638173 is gratefully acknowledged. This research was undertaken at the Micronova Nanofabrication Centre of Aalto University.

[1] S. Nakamura and M. R. Krames, Proc. IEEE **101**, 2211-2220 (2013).
[2] J. Iveland, L. Martinelli, J. Peretti, J. S. Speck and C. Weisbuch, Phys. Rev. Lett. **110**, 177406 (2013).
[3] G. Verzellesi, D. Saguatti, M. Meneghini, F. Bertazzi, M. Goano, G. Meneghesso and E. Zanoni, J. Appl. Phys. **114**, 071101 (2013).
[4] H. Kim, S.-J. Park, H. Hwang and N.-M. Park, Appl. Phys. Lett. **81**, 1326 (2002).
[5] V. K. Malyutenko, S. S. Bolgov and A. D. Podoltsev, Appl. Phys. Lett. **97**, 251110 (2010).
[6] H.-Y. Ryu and J.-I. Shim, Opt. Expr. **19**, 2886–2894 (2011).
[7] C.-K. Li and Y.-R. Wu, IEEE T. Electr. Dev. **59**, 400-407 (2012).
[8] C. A. Hurni, A. David, M. J. Cich, R. I. Aldaz, B. Ellis, K. Huang, A. Tyagi, R. A. DeLille, M. D. Craven, F. M. Steranka and M. R. Krames, Appl. Phys. Lett. **106**, 031101 (2015).
[9] P. Kivisaari, J. Oksanen and J. Tulkki, Appl. Phys. Lett. **103**, 031103 (2013).
[10] L. Riuttanen, P. Kivisaari, H. Nykänen, O. Svensk, S. Suihkonen, J. Oksanen, J. Tulkki and M. Sopanen, Appl. Phys. Lett. **104**, 081102 (2014).
[11] L. Riuttanen, P. Kivisaari, O. Svensk, J. Oksanen and S. Suihkonen, IEEE T. Electr. Dev. **62**, 902–908 (2015).
[12] L. Riuttanen, P. Kivisaari, O. Svensk, J. Oksanen and S. Suihkonen, Appl. Phys. Lett. **107**, 051106 (2015).
[13] J. J. Wierer, D. A. Steigerwald, M. R. Krames, J. J. O'Shea, M. J. Ludowise, G. Christenson, Y.-C. Shen, C. Lowery, P. S. Martin, S. Subramanya, W. Götz, N. F. Gardner, R. S. Kern and S. A. Stockman, Appl. Phys. Lett. **78**, 3379 (2001).
[14] K. Köhler, T. Stephan, A. Perona, J. Wiegert, M. Maier, M. Kunzer and J. Wagner, J. Appl. Phys. **97**, 104914 (2005).
[15] J. Simon, V. Protasenko, C. Lian, H. Xing and D. Jena, Science **327**, 60 (2010).
[16] K. A. Bulashevich, V. F. Mymrin, S. Yu. Karpov, I. A. Zhmakin and A. I. Zhmakin, J. Comput. Phys. **213**, 214 (2006).
[17] E. Kioupakis, Q. Yan and C. G. Van de Walle, Appl. Phys. Lett. **101**, 231107 (2012).
[18] J. Piprek, F. Römer and B. Witzigmann, Appl. Phys. Lett. **106**, 101101 (2015).
[19] M. Goano, F. Bertazzi, X. Zhou, M. Mandurrino, S. Dominici, M. Vallone, G. Ghione, A. Tibaldi, M. Calciati, P. Debernardi, F. Dolcini, F. Rossi, G. Verzellesi, M. Meneghini, N. Trivellin, C. De Santi, E. Zanoni and E. Bellotti, Proc. SPIE **9742**, 974202-1 (2016).
[20] P. Kivisaari, T. Sadi, J. Li, P. Rinke and J. Oksanen, accepted for publication in Adv. Electr. Mat. (2017). DOI: 10.1002/aelm.201600494
[21] R. B. Darling, Phys. Rev. B **43**, 4071 (1991).
[22] M. Boroditsky, I. Gontijo, M. Jackson, R. Vrijen and E. Yablonovitch, J. Appl. Phys. **87**, 3497 (2000).
[23] E. Bellotti and F. Bertazzi, "Transport parameters for electrons and holes" in *Nitride Semiconductor Devices*, edited by J. Piprek (Wiley-VCH, Weinheim, 2007).
[24] J. Geng, P. Sarangapani, E. Nelson, B. Browne, C. Wordelman, T. Kubis and G. Klimeck, Proc. SPIE **10098**, 1009813 (2017).
[25] O. Heikkilä, J. Oksanen and J. Tulkki, J. Appl. Phys. **105**, 093119 (2009).
[26] J. Xue, Y. Zhao, S-H Oh, W. F. Herrington, J. S. Speck, S. P. DenBaars, S. Nakamura, and R. Ram, Appl. Phys. Lett. **107**, 121109 (2015).
[27] J. Oksanen, and J. Tulkki, Nature Photonics **9**, 782 (2015).
[28] P. Santhanam, D. Gray, and R. Ram, Phys. Rev. Lett. **108**, 097403 (2012).
[29] P. Santhanam, D. Huang, R. J. Ram, M. A. Remennyi, and B. A. Matveev., Appl. Phys. Lett. **103**, 183513 (2013).
[30] P. Gibart, Rep. Progress Phys **67**, 667–715 (2004).
[31] A. Tanaka, R. Chen, K. L. Jungjohann, and S. A. Dayeh, Scient. Rep. **5**, 17314 (2015).